Near-Automated Estimate of City Nitrogen Oxides Emissions Applied to South and Southeast Asia

Gongda Lu[1], Eloise A. Marais[1], Karn Vohra[1], Rebekah P. Horner[1], Dandan Zhang[2], Randall V. Martin[2], Sarath Guttikunda[3,4]

[1]Department of Geography, University College London, Gower Street, London, UK.
[2]Department of Energy, Environmental, and Chemical Engineering, Washington University in St. Louis, St. Louis, MO, USA.
[3]Transportation Research and Injury Prevention (TRIP) Center, Indian Institute of Technology, New Delhi, 110016, India.
[4]Urban Emissions, New Delhi, 110016, India.

Corresponding author: Eloise A. Marais (e.marais@ucl.ac.uk)

Key points:

- A refined approach to estimate nitrogen oxides emissions for isolated cities using wind fields and satellite nitrogen dioxide data.
- Many sampling areas defined for each city, increasing success of deriving emissions from 40-60% for one area to 100% for 54 areas.
- Applied to 19 cities in South and Southeast Asia to estimate annual emissions of 23 to 181 kilotonnes in 2019.

Abstract

Cities in South and Southeast Asia are developing rapidly without routine, up-to-date knowledge of air pollutant precursor emissions. This data deficit can potentially be addressed for nitrogen oxides (NO_x) by deriving city NO_x emissions from satellite observations of nitrogen dioxide (NO_2) sampled under windy conditions. NO_2 plumes of isolated cities are aligned along a consistent wind-rotated direction and a best-fit Gaussian is applied to estimate emissions. This approach currently relies on non-standardized selection of the area to sample around the city centre and Gaussian fits often fail or yield non-physical parameters. Here, we automate this approach by defining many (54) sampling areas that we test with TROPOspheric Monitoring Instrument (TROPOMI) NO_2 observations for 2019 over 19 cities in South and Southeast Asia. Our approach is efficient, adaptable to many cities, standardizes and eliminates sensitivity of the Gaussian fit to sampling area choice, and increases success of deriving annual emissions from 40-60% with one sampling area to 100% (all 19 cities) with 54. The annual emissions we estimate range from 16±5 mol s^{-1} for Yangon (Myanmar) and Bangalore (India) to 125±41 mol s^{-1} for Dhaka (Bangladesh). With the enhanced success of our approach, we find evidence from comparison of our top-down emissions to past studies and to inventory estimates that the wind rotation and EMG fit approach may be biased, as it does not adequately account for spatial and seasonal variability in NO_x photochemistry. Further methodological development is needed to enhance its accuracy and to exploit it to derive sub-annual emissions.

Plain Language Summary

Cities are a large source of nitrogen oxides (NO_x) that go on to form many types of air pollutants of harm to human health. City NO_x emissions estimated with observations from space-based instruments are vital in regions that lack access to up-to-date, locally developed inventories. Success of obtaining satellite-derived emissions hinges on user selection of a sampling area around each city centre. Here we present an automated, efficient method that uses many (54) sampling areas. When tested on 19 cities in South and Southeast Asia, annual NO_x emissions are obtained for all 19 cities compared to about half the selected cities when using a single sampling area. With this updated approach, we estimate total NO_x emissions in 2019 that range from 23 kilotonnes for Yangon and Bangalore to almost 10-times more (181 kilotonnes) for Dhaka. The greater success of our updated approach also helps us identify that the accuracy of emissions derivation from satellite observations should be further improved by accounting for the influence of spatial and seasonal variability in NO_x photochemistry.

1 Introduction

Nitrogen oxides ($NO_x \equiv NO_2 + NO$) react to form particulate nitrate and tropospheric ozone and deposit to sensitive habitats (Luo et al., 2019; Sillman, 1999), thus degrading air quality, altering climate, and adversely affecting human health and the environment (Grulke & Heath, 2020; Lelieveld et al., 2015; Yue et al., 2017; Marais et al., 2023). Controls targeting anthropogenic sources of NO_x have been extensively implemented in cities in Europe, the US and China (Curier et al., 2014; de Foy et al., 2016; Silvern et al., 2019). In cities in other parts of the world, particularly South and Southeast Asia, NO_x is increasing rapidly due to fast economic development and limited or absent air quality policies (Vohra et al., 2021; 2022). Vohra et al. (2022) used 14 years of satellite observations of NO_2 from the Ozone Monitoring Instrument (OMI) to infer increases of ~1-14 % a^{-1} in surface NO_2 pollution in almost all rapidly developing large cities in South and Southeast Asia. Only in Jakarta did NO_2 decline due to emission controls applied to vehicles (Vohra et al., 2022). Population projections suggest that, by 2100, one-fifth of the world's most populous cities will be in Southeast Asia (Hoornweg & Pope, 2017), necessitating reliable and up-to-date NO_x emissions estimates for assessing the impact of this growth on urban air quality and for informing air quality policies.

Bottom-up inventories provide estimates of anthropogenic NO_x emissions, but publicly available versions for South and Southeast Asia do not adequately represent contemporary local conditions, as these are derived using outdated activity data, are resource-intensive to produce so lag the present day, are at spatial resolutions that are coarser than many cities in the region, and data needed to compile the inventories do not exist for many countries (Kurokawa & Ohara, 2020). The two most used bottom-up inventories for these regions are the Regional Emission inventory in Asia (REAS) (Kurokawa & Ohara, 2020) and the inventory known as MIX, a mosaic of REAS and other regional inventories (Li et al., 2017). REAS and MIX are at ~25 km resolution, MIX only covers 2 years of data, and the most recent years are 2015 for REAS and 2010 for MIX. Still, REAS and inventories used to create MIX are routinely incorporated in global inventories such as the Community Emissions Data System (CEDS$_{\text{GBD-MAPS}}$) (McDuffie et al., 2020), and Hemispheric Transport of Air Pollution (HTAP) (Crippa et al., 2023).

Independent and contemporary estimates of city NO_x emissions can be derived with satellite observations of tropospheric NO_2 vertical column densities (VCDs) without the need for resource-intensive computer models. A method first proposed by Beirle et al. (2011) involves selecting isolated cities and treating these as large point sources of NO_x. In this approach, individual satellite pixels within a target domain centred on a city centre were split into eight major wind directions to resolve the city plume in each direction. A mathematical function was then fit to the plume to account for its Gaussian shape and exponential decay of NO_2. This fit, referred to as an Exponential Modified Gaussian (EMG), yields parameters that are then used to estimate NO_x emissions. It also yields an effective lifetime of NO_x for the city plume that is dominated by dispersion for the windy conditions sampled. As dispersion dominates, the derived lifetime is much shorter than the chemical lifetime of NO_x that includes conversion to nitric acid (HNO_3) or organic nitrates (de Foy et al., 2014; Laughner & Cohen, 2019) and, to a lesser extent, dry deposition of NO_2 (Zhang et al., 2012). Beirle et al. (2011) used OMI observations of NO_2 to derive NO_x emissions for eight global megacities. The Beirle et al. (2011) approach required many (four) years of OMI data to achieve distinct plumes in each wind direction.

Valin et al. (2013) expanded on the approach developed by Beirle et al. (2011) by demonstrating that all satellite data can instead be aligned along a single upwind-downwind direction relative to the city centre. This approach reduced the number of observations needed to distribute the data by wind direction and so extended application to a greater number of geographically isolated cities over shorter sampling periods. Wind rotation of OMI observations and the EMG fit have since been used to calculate city NO_x emissions predominantly in the US (de Foy et al., 2014; Goldberg et al., 2019a; Lu et al., 2015) and for select cities worldwide (Goldberg et al., 2021). Following the 2017 launch of the higher spatial resolution TROPOspheric Monitoring Instrument (TROPOMI), the wind rotation, EMG fit, and related approaches have been extended to smaller isolated cities and shorter sampling periods than was possible with OMI. Applications include cities in western Europe (Lorente et al., 2019; Pope et al., 2022), China (Wu et al., 2021), the US (Goldberg et al., 2019b), and worldwide (Lange et al., 2022), as well as investigating changes in NO_x emissions due to COVID-19 lockdown measures in the New York Metropolitan Area (Tzortziou et al., 2022) and for select cities in India, Argentina, and Spain (Lange et al., 2022). So far, the wind rotation and EMG fit has only been applied to 5-13 cities in South and Southeast Asia as part of global studies (Goldberg et al., 2021; Lange et al., 2022).

Even though there has been substantial development and use of the EMG fit, it still requires that a user define a sampling area around the city that effectively captures the wind rotated plume. The area selected varies with city size and plume length (Lu et al., 2015; Goldberg et al., 2019a; Lange et al., 2022). This approach often yields no or poor EMG fits and non-physical best-fit parameters (Laughner & Cohen, 2019), decreasing the likelihood of deriving top-down emissions. Selecting appropriate city-specific areas for the wide-ranging city sizes in South and Southeast Asia is also time consuming and not standardized.

Here we develop a near-automated and efficient EMG fitting routine for deriving annual city NO_x emissions, demonstrate the utility of this automation by applying it to TROPOMI NO_2 observations over isolated cities in South and Southeast Asia with wide-ranging city sizes, compare our top-down emissions to past studies and a global bottom-up inventory, and exploit the greater success of our updated sampling to identify opportunities to further develop the EMG fit approach.

2 Materials and Methods

2.1 TROPOMI NO_2 and City Selection

We use Level 2 TROPOMI NO_2 tropospheric column VCDs for 2019 from the Sentinel-5P Products Algorithm Laboratory (S5P-PAL) portal (https://data-portal.s5p-pal.com/; last acquired 30 January 2022). These data have been retrieved with a consistent algorithm (version 02.03.01) and corrected for a low bias in NO_2 over polluted scenes (Eskes et al., 2021). TROPOMI achieves daily global coverage with a swath width of 2600 km, an equator crossing time of 13:30 local solar time (LST), and a nadir pixel resolution that increased on 5 August 2019 from 7 km × 3.5 km to 5.5 km × 3.5 km. We use cloud-free, high-quality data identified with a quality flag ≥ 0.75 (van Geffen et al., 2021).

To identify isolated cities appropriate for top-down estimate of NO_x emissions, we first oversample TROPOMI NO_2 to obtain high-resolution gridded annual means (0.05° × 0.05°; ~6 km latitude × ~5 km longitude) by weighting areas of overlap between the satellite pixels and cells on a fixed latitude-longitude grid using tessellation (Sun et al., 2018). We use the resultant gridded TROPOMI NO_2 shown in Figure 1 to manually select 19 cities that are isolated hotspots. The 19 selected cities are Karachi, Islamabad, and Lahore in Pakistan; Kabul in Afghanistan; Ahmedabad, Mumbai, Delhi, Bangalore, Chennai, and Kolkata in India; Colombo in Sri Lanka; Dhaka in Bangladesh; Yangon in Myanmar; Bangkok in Thailand; Kuala Lumpur in Malaysia; the sovereign city Singapore; Ho Chi Minh City in Vietnam; Jakarta in Indonesia; and Manila in the Philippines. Other hotspots in Figure 1 are either not cities, such as the coal-fired power plants concentrated in eastern India, or are not isolated, such as Hanoi, Haiphong and Nam Dinh in northern Vietnam.

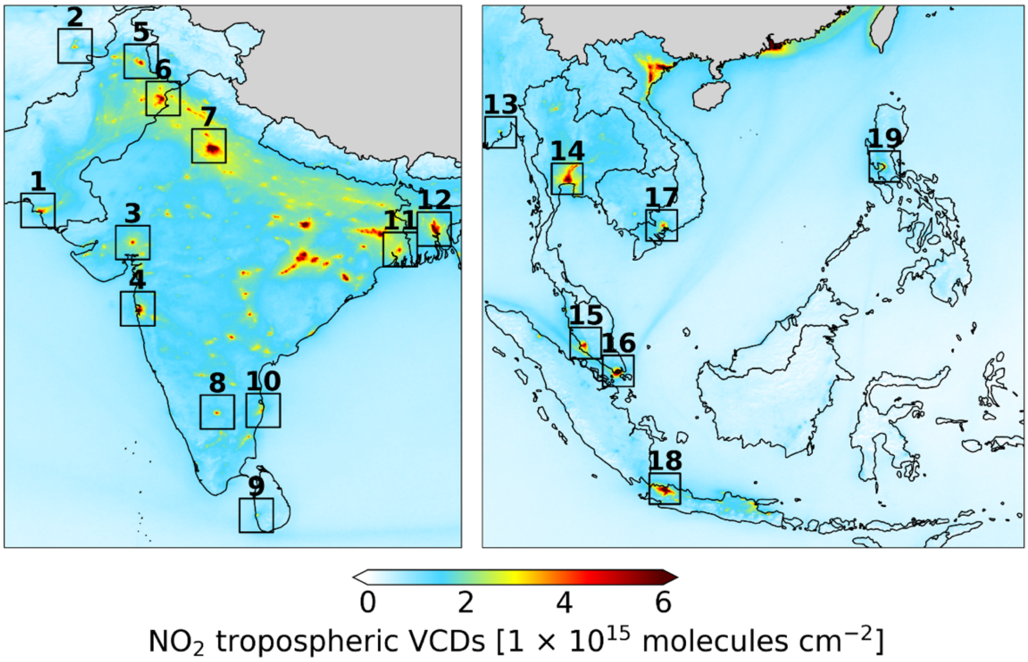

Figure 1. Annual mean TROPOMI tropospheric NO_2 VCDs over South and Southeast Asia in 2019. Maps show South (left) and Southeast (right) Asia TROPOMI NO_2 oversampled to 0.05° × 0.05°. The 19 selected cities, numbered from east to west, are Karachi (1), Islamabad (5), and Lahore (6) in Pakistan; Kabul (2) in Afghanistan; Ahmedabad (3), Mumbai (4), Delhi (7), Bangalore (8), Chennai (10), and Kolkata (11) in India; Colombo (9) in Sri Lanka; Dhaka (12) in Bangladesh; Yangon (13) in Myanmar; Bangkok (14) in Thailand; Kuala Lumpur (15) in Malaysia; the sovereign city Singapore (16); Ho Chi Minh City (17) in Vietnam; Jakarta (18) in Indonesia; and Manila in the Philippines (19).

2.2 Wind Rotation and EMG Fit

Figure 2 illustrates the major steps involved in the wind rotation and EMG fit to derive annual NO_x emissions for Singapore. The wind fields we use to calculate wind direction and speed to retain TROPOMI NO_2 observations under windy conditions are the fifth generation European ReAnalysis (ERA5) 3D hourly *u* and *v* wind components (https://cds.climate.copernicus.eu/cdsapp#!/home; last acquired 18 March 2022) provided at 0.25° × 0.25° resolution. At each TROPOMI NO_2 pixel, we compute collocated mean ERA5 wind speeds and directions 30 min around 13:30 LST, the TROPOMI overpass time, in the lowest 5 layers (≥ 900 hPa) to capture dispersion of mixed-layer near-surface NO_2 plumes. Within a 4° × 4° domain around each city centre, we isolate TROPOMI pixels with coincident wind speeds > 2 m s^{-1}, the threshold typically used for windy conditions (Beirle et al., 2011; Pope et al., 2022). We rotate each TROPOMI NO_2 pixel by the angle of its wind direction, preserving the distance of the pixel from the city centre. This aligns all pixels along the same "upwind-downwind" direction that in our work is from north to south (Figure 2(a)). After wind rotating all pixels in a year (as in Figure 2), we grid pixels onto a uniform 0.05° × 0.05° grid using simple point-in-box averaging (Figure 2(a)) and fill empty grid cells (grey squares in Figure 2(a)) using nearest-neighbour interpolation to reduce low biases in the steps that follow.

Next, the 2D map in Figure 2(b) is converted to 1D line densities by summing all grid cells in the across-wind (east-to-west) direction in 0.05° upwind-downwind (north-to-south) increments. In the standard approach, a single area smaller than the 4° × 4° domain is used, defined by the distance upwind, downwind, and across-wind of the city centre. Instead of using a single area, we define multiple areas that encompass the range of sizes typically used in past studies (Goldberg et al., 2021; Lange et al., 2022; Laughner & Cohen, 2019). These, defined as distances from the city centre, are 0.5°, 0.75°, and 1° upwind, 0.5°, 0.75°, 1.0°, 1.25°, 1.5°, 1.75°, 2.0° downwind, and 0.5°, 0.75°, and 1.0° across-wind, with the requirement that the distance downwind of the city centre is ≥ the distance upwind to capture the extent of the city plume. This yields 54 areas and associated line densities. The sizes of the smallest and largest areas sampled and the across-wind 0.05° increments summed to obtain line densities in the smallest area sampled are shown in Figure 2(b).

The EMG model we use to fit to the observed 1D line densities is the Laughner & Cohen (2019) formulation:

$$F(x|a, x_0, \mu_x, \sigma_x, B) = \frac{a}{2x_0} \exp\left(\frac{\mu_x}{x_0} + \frac{\sigma_x^2}{2x_0^2} - \frac{x}{x_0}\right) \operatorname{erfc}\left(-\frac{1}{\sqrt{2}}\left[\frac{x-\mu_x}{\sigma_x} - \frac{\sigma_x}{x_0}\right]\right) + B \quad (1),$$

where x is the distance of each line density upwind and downwind of the city centre (Figure 2(c)) and a, x_0, μ_x, σ_x and B are best-fit parameters. Of these, a is total NO_2 in the plume (in moles), x_0 is the *e*-folding distance or length scale of NO_2 decay (in km), μ_x is the location of the apparent source relative to the city centre (in km) or the peak of the Gaussian fit that in Figure 2(c) is located ~20 km downwind or south of the city centre, σ_x is the Gaussian smoothing length scale (in km) that is ~2.355 × the Full Width at Half Maximum (FWHM), and B is background NO_2 (in moles m^{-1}).

We use initial guesses for the best-fit parameters in Equation (1) that are similar to those from Laughner & Cohen (2019), but our fitting procedure differs. Laughner & Cohen (2019) used a non-linear interior point minimization algorithm (the *fmincon* function in MATLAB) to optimize model parameters with 10 iterations per line density. Instead, we perform the fit with the *scipy.optimize.curve_fit* module from SciPy Python package version 1.7.3 and iterate on the fit until the difference in fitting parameters between the current and previous iteration is negligible (< 0.001%) for at most 10 iterations. Fit convergence is usually achieved after 3 iterations. Only good-quality fits are retained, identified with goodness-of-fits (R^2) > 0.8, as in Laughner & Cohen (2019). We further screen for physically implausible best-fit parameters using criteria similar to Laughner & Cohen (2019): a is positive, x_0 is at least 1.6 km (approximately 1/*e* of the grid resolution), μ_x is within the sampling area, the emission width is less than the *e*-folding distance ($\sigma_x < x_0$), background NO_2 is positive and less than the maximum line density value, and the *e*-folding distance occurs between the plume centre and the edge of the sampling area. We introduce an additional requirement to ensure that x_0 is within the sampling area (x_0 < length of sampling area downwind of the city centre).

The Singapore example in Figure 2 is an ideal city, as all 54 EMG fits are successful. Figure 2(c) shows that the observed line densities are most sensitive to the across-wind length, as this determines the amount of NO_2 summed to yield each line density. We will demonstrate in Section 3 that for many of the cities in Figure 1 a large number of EMG fits fail to meet the conditions for success, necessitating as many as 54 fits.

The successful EMG fits are used to calculate effective NO_x lifetimes (τ_{NO_x}; reported in h) and midday NO_x emissions (E_{NO_x}; in moles s^{-1}):

$$\tau_{NO_x} = \frac{x_0}{\omega} \quad (2)$$

$$E_{NO_x} = \gamma \times \frac{a}{\tau_{NO_x}} \quad (3),$$

where ω is the sampling area mean wind speed (in m s^{-1}) and γ is the unitless molar ratio of $[NO_x]/[NO_2]$ to convert moles NO_2 to moles NO_x. The up to 54 individual estimates of τ_{NO_x} and E_{NO_x} are averaged to obtain values for each city.

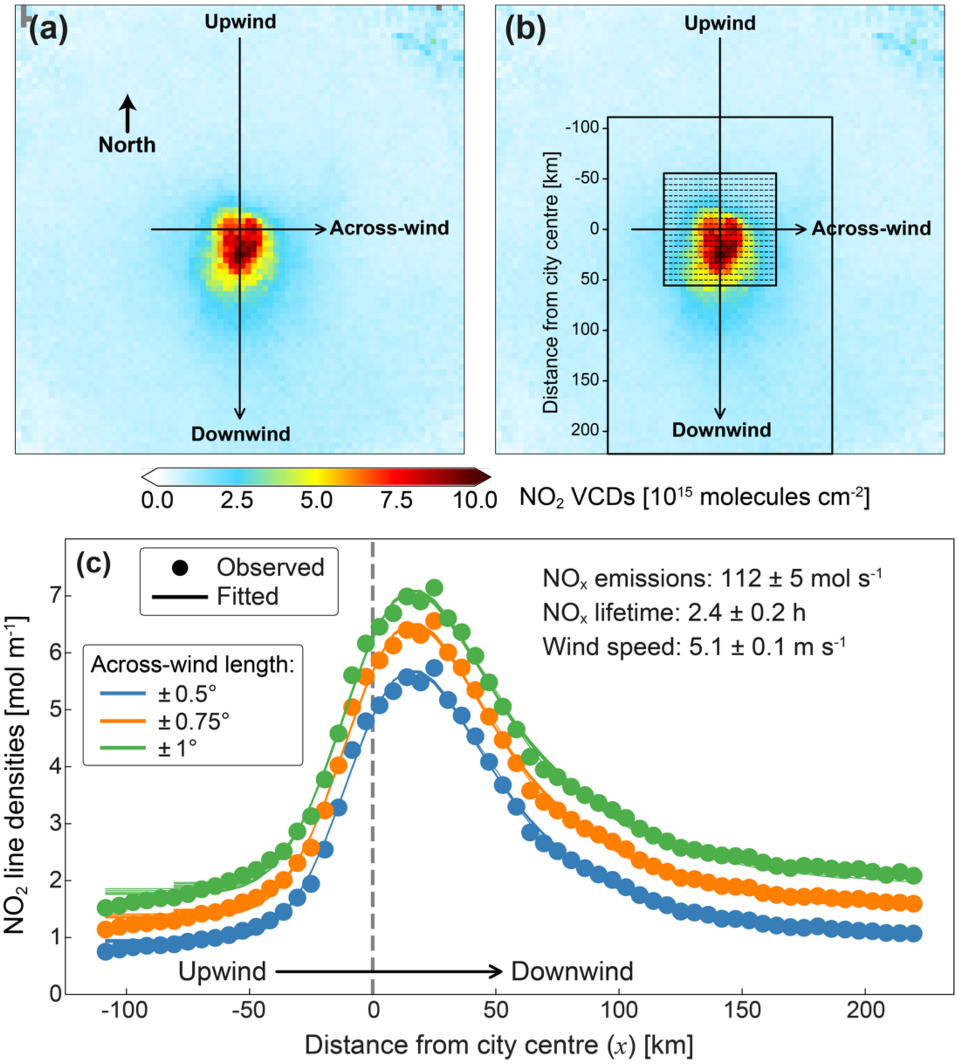

Figure 2. Illustration of major steps in the wind rotation and EMG fit to derive annual NO_x emissions for Singapore. The main steps in each panel are wind rotate and grid windy scene TROPOMI NO_2 pixels to 0.05° × 0.05° (a), fill data gaps (b), and fit the EMG function (Eq. (1)) (solid lines) to observed line densities (filled circles) (c). In (b), black rectangles show the extent of the largest and smallest sampling areas and dashed lines in the smallest area show the 0.05° increments used to calculate the line densities in (c). All 54 successful EMG fits, 18 lines for each of the three across-wind lengths, are shown in (c). Values in (c) give the mean and standard deviation of the city NO_x emissions (Eq. (3)), effective NO_x lifetime (Eq. (2)), and sampling area ERA5 wind speed. The goodness-of-fit (R^2) is ≥ 0.99 for all fits in (c).

We use the same $[NO_x]/[NO_2]$ = 1.32 value as Beirle et al. (2011) and subsequent studies to represent rapid cycling between NO and NO_2. Liu et al. (2022) determined with synthetic experiments that city NO_x emissions are relatively unaffected by variability in $[NO_x]/[NO_2]$, but that study was for US cities. Surface measurements aid in determining suitability of $[NO_x]/[NO_2] = 1.32$, but these are limited to cities in India and have data quality issues (Vohra et al., 2021). Instead, we use the GEOS-Chem model to assess suitability of the 1.32 value. We simulate the model in 2019 and sample the lowest model layer around the TROPOMI overpass time. We use output from a coarse and finer resolution version of GEOS-Chem to also test sensitivity of this ratio to model resolution, especially given many of these cities are coastal (Figure 1). We use the classical configuration of the model that operates on a single computational node, called GEOS-Chem Classic (GCClassic), and the high-performance model configuration (GCHP) that is a parallelized across multiple computational nodes to enable finer resolution global simulations (Eastham et al., 2018). GCClassic is version 13.3.4 (https://doi.org/10.5281/zenodo.5764874) run on a fixed 2° × 2.5° global grid and GCHP is version 13.4.1 (https://doi.org/10.5281/zenodo.6564711) run on a C360 global grid (~25 km × ~31 km). GCClassic and GCHP use the same vertical grid and chemical mechanism. For GCClassic, grid squares that overlap with each city are sampled, whereas for GCHP, we use city sampling extents determined from a combination of administrative and geographic boundary shapefiles and Google Maps (Figure S1). Midday sampling is at 12:00 to 15:00 LST from GCClassic and 13:00 to 14:00 LST from GCHP. At midday, NO_x is in photochemical steady state, so the relative abundance of NO and NO_2 is insensitive to the extent of the sampling window around midday (Potts et al., 2021).

We calculate uncertainties in the NO_x emissions by adding individual errors in quadrature. These include best-fit parameters x_0 and a, sampling area mean wind speed ω, the TROPOMI NO_2 observations, and $[NO_x]/[NO_2]$. We use the relative standard deviation from all successful EMG fits to calculate city-specific errors in x_0 and a. For ω, we consider errors due to the choice of spatial and temporal sampling and the threshold used for windy conditions. We use the Beirle et al. (2011) estimated 10% error in temporal sampling choice and 5% error due to vertical sampling choice. We conduct our own tests of the sensitivity to threshold and spatial sampling choice. For $[NO_x]/[NO_2]$ we assess whether the 10% error attributed to this variable by Beirle et al. (2011) is appropriate by quantifying the percent deviation of GCClassic and GCHP $[NO_x]/[NO_2]$ from 1.32. Beirle et al. (2011) applied a 30% error to OMI that is also appropriate for TROPOMI. Even though uncertainties in TROPOMI slant columns (NO_2 along the viewing path) are much less than those from OMI (van Geffen et al., 2020), the air mass factor used to convert slant columns to VCDs remains the largest contributor to errors in NO_2 VCDs and is similar for OMI and TROPOMI (van Geffen et al., 2021).

2.3 Bottom-up Anthropogenic Emissions

We compare our top-down estimates to anthropogenic NO_x emissions from the widely used bottom-up HTAP inventory version 3 (HTAP_v3) (Crippa et al., 2023). HTAP_v3 has high enough spatial resolution (0.1° × 0.1°) to resolve cities selected in Figure 1. The most recent year is 2018, achieved by extending emissions from the regional REAS inventory ending in 2015 to the year 2018 with trends from the Emissions Database for Global Atmospheric Research (EDGAR) inventory. The same sampling boundaries as GCHP are used (Section 2.2; Figure S1). The HTAP_v3 NO_x emissions include contributions from aviation, transport (road, rail, pipeline, inland waters), shipping, energy, industry, and residential sectors.

Cities targeted can be influenced by non-anthropogenic NO_x sources, such as open burning of biomass (Marvin et al., 2021) and natural sources such as soils (Weng et al., 2020) and lightning (Miyazaki et al., 2014). We assess suitability of comparing our top-down emissions to anthropogenic bottom-up emissions only by determining the percent contribution of anthropogenic emissions to total NO_x emissions. To do this, we simulate total NO_x emissions with the Harmonized Emissions Component (HEMCO) standalone model version 3.0.0 (https://zenodo.org/records/4984639; last accessed 20 March 2022) (Lin et al., 2021) and sample the same spatial extent as GCHP and HTAP_v3 (Figure S1). HEMCO is run at a spatial resolution of 0.25° × 0.3125° (~ 28 km latitude × ~ 33 km longitude). HEMCO calculates open biomass burning emissions using the Global Fire Emissions Database with small fires (GFED4s) inventory (Randerson et al., 2017) and reads in and processes lightning and soil NO_x from offline emissions at the same resolution as HEMCO (Murray et al., 2012; Weng et al., 2020).

Bottom-up emissions from HTAP_v3 are 24-h means, whereas top-down estimates derived using TROPOMI are representative of midday emissions. Goldberg et al. (2021) multiplied satellite-derived midday NO_x emissions by 0.77 to convert midday top-down NO_x emissions to 24-h means for comparison to bottom-up inventories. This value was inferred from bottom-up emissions estimates for the Netherlands, so may not be suitable for the selected cities in South and Southeast Asia. The hourly scaling factors used by HEMCO for the chosen cities range from 0.70 to 1.16. These are for the year 2000 and are extrapolations of values for conditions in Europe, so may not be suitable for the year and cities targeted in this study. Given this, we do not scale top-down emissions and instead discuss whether differences in averaging times contribute to discrepancies between top-down and bottom-up emissions estimates.

3 Results and Discussion

3.1 Wind Rotation and EMG Fit Metrics

Isolating windy condition (> 2 m s^{-1}) satellite pixels removes 8-34% of all 2019 quality- and cloud-screened TROPOMI NO_2 pixels for most cities in Figure 1. Cities with greater data loss are Lahore (43% data loss), Kabul (58%) and Islamabad (63%). No spatial data gap filling (Section 2.2, Figure 2) is needed within the areas sampled, due to the high sampling frequency of TROPOMI. If only a single domain size is selected, annual EMG fits meet all criteria for success for 7 to 12 of the 19 cities in Figure 1, depending on the sampling area chosen. Using our extended method, we successfully derive annual NO_x emissions for all 19 cities, due to the enhanced probability of obtaining at least one successful EMG fit.

Figure shows the number of successful EMG fits (orange bars) range from 3 (Kabul) to all 54 (Singapore). Singapore, Dhaka, Jakarta, Karachi, Manila, and Mumbai are least impacted by the choice of sampling area. The 6 cities in Figure 3 with < 20 fits are most likely to fail if only a single sampling area is used. For all retained EMG fits, differences between observed and fitted NO_2 line densities, the fit residuals, are negligible. The most common causes for a failed EMG fit rank as: background NO_2 (B in Equation (1)) > maximum NO_2 line density (36% of all fits conducted), $R^2 \leq 0.8$ (24%), emission width > e-folding distance (19%), total plume NO_2 (a in Equation (1)) < 0 (13%), and e-folding distance > the downwind length of the sampling area (12%). Multiple causes can co-occur in a single fit, so cumulative percentages exceed 100%.

We also test sensitivity of top-down NO_x emissions to the choice of wind speed threshold and horizontal sampling extent to attribute an error to these. For this, we apply a stricter wind speed threshold of 3 m s^{-1} and test the difference in NO_x emissions if instead of filtering for windy conditions using pixel-mean wind fields, we calculate a sampling-area mean wind speed to filter for windy conditions as in Goldberg et al. (2019a). We apply these conditions to a mid-sized sampling area of 0.75° upwind, 1.5° downwind, and ±0.75° across-wind. Variability in NO_x emissions for cities with successful EMG fits for all 4 wind sampling conditions is at most 10% (Figure S2). Given these results, we attribute a 10% error to the choice of horizontal sampling and to the wind speed threshold.

GCClassic (coarse resolution) annual mean [NO_x]/[NO_2] for the target cities ranges from 1.25 (Dhaka) to 1.41 (Kabul). The range in ratios from GCHP (finer resolution) is wider at 1.24 (Ahmedabad) to 1.64 (Kolkata). The difference in ratios between the coarse and fine resolution models is typically ±10%, except for a few cities with ratios from the fine resolution model that exceed the coarse resolution model by 14% for Singapore, 16% for Lahore, 23% for Dhaka, and 23% for Kolkata. This is because the fine resolution model better resolves the city plume that includes a greater proportion of NO_x as NO from fresh emission sources. As the difference between the model city ratios and the 1.32 value is ±10% for most cities, we use the same 10% error for [NO_x]/[NO_2] as Beirle et al. (2011).

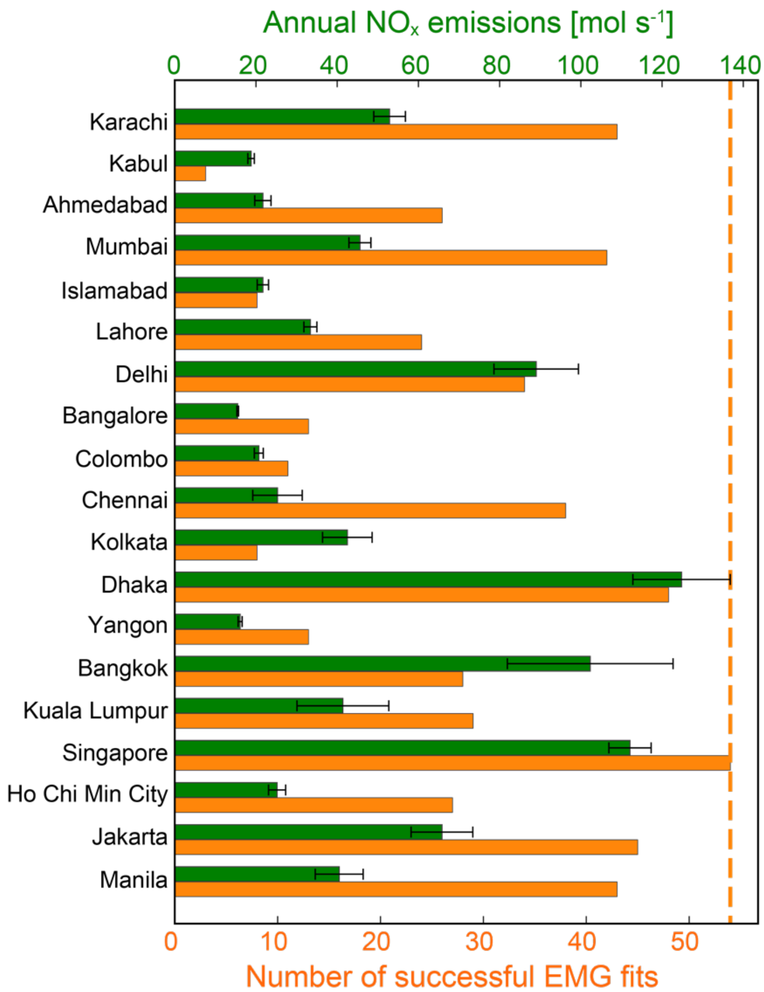

Figure 3. Successful EMG fits and top-down NO_x emissions for the cities targeted in this study. Bars are emissions (green) and the corresponding number of successful fits (orange). Black error lines are NO_x emission standard deviations for all successful fits. The orange dashed line at 54 indicates the maximum possible EMG fits. Emissions multiplied by ~1.45 yields emissions in Gg NO_2 a^{-1}.

3.2 Top-Down NO_x Emissions

Green bars in Figure 3 show the mean annual top-down NO_x emissions for all cities (values are in Table S1). These range from ~16 mol s^{-1} for Bangalore and Yangon to ~125 mol s^{-1} for Dhaka. The range in the total mass of NO_x emitted for these cities, assuming the midday emission rate is reasonably representative of the 24-h emission rate, is 23-181 Gg NO_x as NO_2. Emissions for most cities are < 50 mol s^{-1} (<73 Gg NO_x as NO_2 a^{-1}). Cities with emissions between 50-100 mol s^{-1} (73-145 Gg NO_x as NO_2 a^{-1}) include Karachi, Delhi, and Jakarta and > 100 mol s^{-1} (> 145 Gg NO_x as NO_2 a^{-1}) include Bangkok, Singapore, and Dhaka. Emission rates for Bangkok, Dhaka and Singapore are comparable to the range of top-down emissions estimated for large, polluted cities in China using the EMG approach (Wu et al., 2021). The effective lifetimes for the cities in Figure 1 (shown in Figure S3) range from 1.2 h for Colombo to 6.3 h for Kuala Lumpur. Variability in effective lifetimes depends most strongly on the downwind extent of the plume. The Pearson's correlation coefficient, R, between city mean effective lifetimes and x_0 values is 0.90.

For the target cities, the relative standard deviations of annual NO_x emissions (black error lines in Figure 3) range from just 1% for Bangalore to 27% for Kuala Lumpur. This is far less than the equivalent Gaussian fit uncertainty of 10-50% estimated by Beirle et al. (2011) for a single sampling area. The relatively large variability in Kuala Lumpur NO_x emissions is because the smaller EMG sampling areas do not fully encompass the elongated wind rotated city NO_2 plume, causing a low bias in NO_x emissions for the smaller areas sampled. The effect of this is dampened by the almost 30 successful fits used to obtain mean NO_x emissions for this city. The relative standard deviations of the NO_x lifetimes (Figure S3) range from 3% for Bangalore to 37% for Chennai. The relative standard deviations of other parameters are ~6% for wind speeds (Figure S4), 4% (Bangalore) to 38% (Chennai) for x_0, and 4% (Kabul and Bangalore) to 37% (Bangkok) for *a*.

The overall uncertainty in annual NO_x emissions we obtain by adding all error contributions in quadrature ranges from 32% for Bangalore and Yangon to 55% for Bangkok. Values for all cities are in Table S1. The TROPOMI NO_2 VCDs make the largest contribution to the overall uncertainty. The higher-end of our uncertainty estimates is similar to the typical ~50% uncertainty reported in past studies (Beirle et al., 2011; Verstraeten et al., 2018; Goldberg et al., 2021). We use our overall uncertainties in the comparison of our top-down emissions to values from the literature and from HTAP in the sections that follows.

3.3 Comparison to Top-Down Estimates from Past Studies

To assess our approach, we compare in Figure 4 our annual NO_x emissions to values from past studies that used similar sampling time periods and a single sampling area. These include multiyear (2017-2019) mean emissions from Goldberg et al. (2021) obtained using the OMI sensor and emissions from Lange et al. (2022) obtained with select days of TROPOMI data from 2018 to 2020. Goldberg et al. (2021) estimated emissions for 10 of the 19 cities in our study. These we read from their Figure S10 for Karachi, Figure S11 for 4 cities in India, and Figure S13 for 5 cities in Southeast Asia and divide by the 0.77 midday to 24-h scaling factor used in that study. Emissions are reported by Lange et al. (2022) for 5 of the 19 cities in our study. Based on the regression statistics in Figure 4, our emissions are typically ~26% more than estimates from these past studies. Exceptions are Mumbai, Ahmedabad, and Chennai that in our study are 16-29% less than Goldberg et al. (2021). Lange et al. (2022) used an earlier version of the TROPOMI data product that has a known low bias in NO_2 VCDs over very polluted scenes (van Geffen et al., 2022). Differences in TROPOMI data products are the likely cause for our higher Delhi (by 27%) and Singapore (by 18%) emissions. Relatively small error estimates from Lange et al. (2022) are because they only propagate error contributions from the wind speed data and the EMG fit.

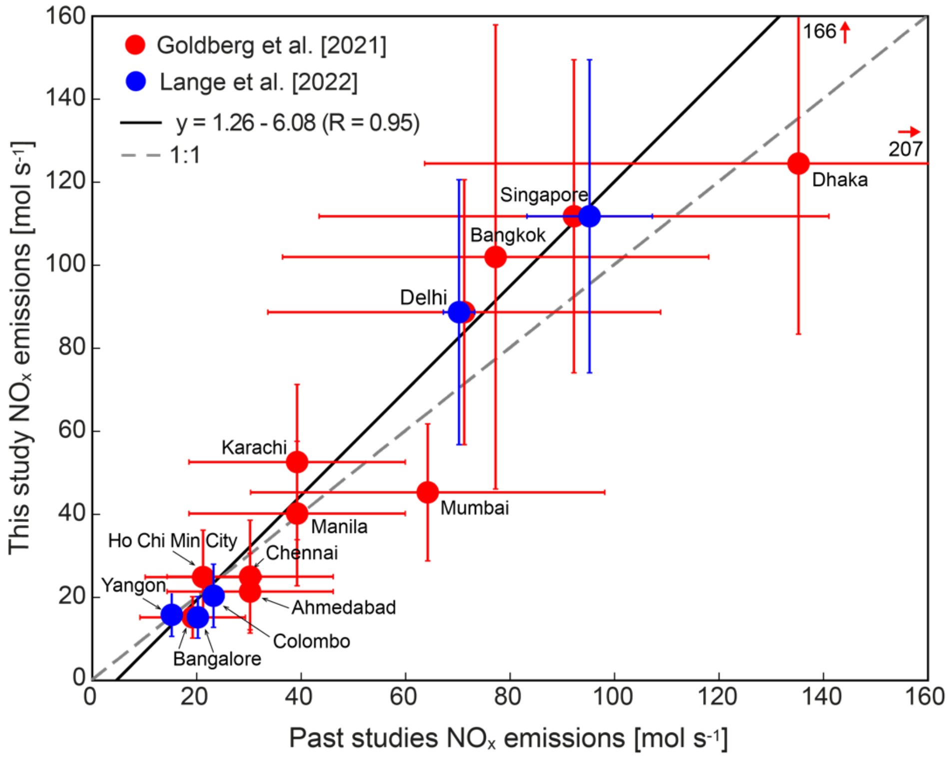

Figure 4. Comparison of our and past top-down NO_x emissions. Symbols compare our emissions to those from Goldberg et al. (2021) (red) and Lange et al. (2022) (blue). Error bars are overall uncertainties for our study (Section 2.2, Table S1), the same 53% uncertainty applied to all cities by Goldberg et al. (2021) and the city-specific uncertainties for Lange et al. (2022). Lines are the Theil regression fit (solid black) and 1:1 relationship (dashed grey). Inset text gives the regression statistics and Pearson's correlation coefficient (R). Arrows and inset text for Dhaka give the error values that extend beyond the plotting range.

Discrepancies between Goldberg et al. (2021) and our emissions are not as straightforward to diagnose, as Goldberg et al. (2021) use NO_2 VCDs from a different sensor (OMI) and apply a systematic 37% increase to NO_x emissions to correct for a low bias in OMI attributed to the coarse resolution a priori used in the NO_2 VCDs retrieval. Sampling area choice may also be a factor. For example, the smallest of our 54 areas yields NO_x emissions of 102 mol s^{-1} for Singapore that is 10 mol s^{-1} less than the mean of all EMG fits. Goldberg et al. (2021) used year-round OMI data for all cities except Delhi and Karachi. As these cities are north of 25°N, only May-September observations were used by Goldberg et al. (2021). We find that Delhi and Karachi mean May-September TROPOMI NO_2 VCDs in 2019 averaged within the 4° × 4° domain selected for each city (Figure 2(a)-(b)) are 11-12% less than those in October-April, due to the shorter photochemical lifetime of NO_x in the warmer months. Open biomass burning emissions also influence seasonality in the TROPOMI NO_2 VCDs, but the EMG fit accounts for this by distinguishing background NO_2 (*B* in Equation (1)) from NO_2 in the city plume (*a* in Equation (1)).

We find that if we apply the EMG fit to individual months for Delhi and Karachi, all 54 EMG fits fail for Delhi in July-August and yield spurious results in September due to large data loss resulting from persistent clouds during the monsoon season. All 12 months are retained for Karachi, Singapore and Manila. November-April mean values of *a* are 21% more than in May-October for Karachi, 9% more for Singapore, and 39% more for Manila. This suggests that using NO_2 VCDs for a portion of the year may yield systematic biases in emissions that may not reflect seasonality in the underlying activities affecting the emissions. Larger wintertime than summertime emissions have also been reported in the global study of Lange et al. (2022). They quantified summer-to-winter emission ratios of ~0.5 for Colombo and Delhi. The top-down emissions calculation (Equation (3)) does not fully account for seasonality in photochemistry. The derived effective NO_x lifetimes used to calculate NO_x emissions (Equation (2)) are mostly influenced by dispersion. As a result, the effective lifetimes are much shorter than the expected chemical lifetimes of NO_x (de Foy et al., 2014). In the synthetic experiment scenarios tested by de Foy et al. (2014), the EMG fit applied to wind rotated data yielded an effective lifetime of 4 h for a 12-h chemical lifetime scenario. According to Shah et al. (2020), the chemical lifetime of NO_x for central-eastern China centred at ~35°N, the northerly portion of our domain, ranges from ~6 h in summer to ~24 h in winter. None of the monthly effective lifetimes for our target cities reproduces this seasonality and the longest lifetime is 13.3±3.7 h for Yangon in November. The implication is that the size of absolute emissions derived with sub-annual satellite data may be biased, but should have negligible effect if used to quantify relative trends, as in Goldberg et al. (2021) and Laughner & Cohen (2019), for example.

3.4 Comparison to Bottom-up Emissions

Figure 5 compares annual top-down and bottom-up NO_x emissions. According to our HEMCO simulations, anthropogenic sources account for most (>87%) annual NO_x emissions. The relative differences between our top-down estimates and the bottom-up inventory are within 50% for Mumbai (1%), Bangkok (2%), Chennai (9%), Ahmedabad (11%), Kolkata (21%), Singapore (21%), Bangalore (32%), Manila (35%), and Kuala Lumpur (46%). A 50-100% difference occurs for Ho Chi Minh City (53%), Jakarta (54%), Delhi (64%), and Colombo (91%). Even greater relative differences occur for Karachi (2.1 times), Islamabad (2.1 times), Lahore (2.4 times), Yangon (3.3 times), Dhaka (6.9 times), and Kabul (11-fold). The largest absolute discrepancies are for Dhaka and Jakarta. Bottom-up emissions are 107 mol s^{-1} less than the top-down values for Dhaka and 78 mol s^{-1} more for Jakarta. On a mass basis, this is equivalent to a 155 Gg NO_x as NO_2 underestimate for Dhaka and a 113 Gg NO_x as NO_2 overestimate for Jakarta.

The different years used (2018 for HTAP, 2019 for TROPOMI) should at most account for a 14% difference in emissions, based on the size of annual trends inferred by Vohra et al. (2022) using long-term observations of OMI NO_2 VCDs over large and fast-growing cities in South and Southeast Asia. Vohra et al. (2022) identified that emission inventories do not capture the steep decline in NO_x emissions in Jakarta attributed to national policies targeting vehicles. In addition to misrepresenting annual changes in underlying activities, the emission factors are mostly informed by studies in China and Japan (Kurokawa & Ohara, 2020). The bottom-up and top-down emissions differences for many cities also exceed the ±30% difference that results from the choice of bottom-up emissions grid sampling and the ±30% difference from the timing of the top-down (midday) and bottom-up (24-h) estimates inferred by Goldberg et al. (2021).

Apparent in Figure 5 is a latitudinal pattern in the discrepancies. Top-down emissions are greater than bottom-up emissions for cities to the north and vice versa for cities to the south, so that in general top-down emissions exceed bottom-up emissions in South Asia and vice versa in Southeast Asia. NO_x chemical loss varies with latitude, due to variability in the amount of sunlight available to form hydroxyl and peroxy radicals required to form HNO_3 and organic nitrates, the main daytime chemical loss pathway for NO_x. This latitudinal pattern is likely because the EMG fit also does not fully account for spatial variability in NO_x photochemistry, imparting a bias in the top-down emissions. The size of this bias will depend on the relative contribution of NO_x chemical loss to total loss in the wind rotated plume.

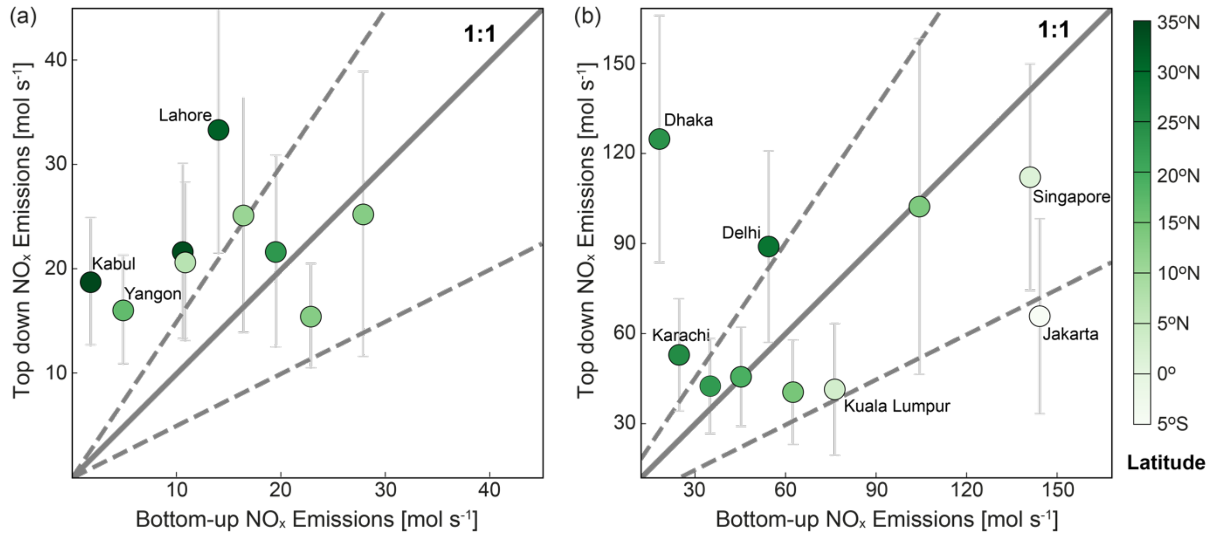

Figure 5. Comparison of annual top-down and bottom-up NO_x emissions for target cities. Data are coloured by city centre latitude and split into top-down NO_x emissions < 40 mol s^{-1} (a) and ≥ 40 mol s^{-1} (b). Error bars are the overall uncertainty in top-down emissions estimates. Grey lines indicate 1:1 agreement (solid) and ±50% difference (dashed). The bottom-up emissions sampling extent of each city is in Figure S1. Data used to generate the figure are in Table S1.

4 Conclusions

City nitrogen oxides (NO_x) emissions can be derived with a now well-established approach using satellite observations of nitrogen dioxide (NO_2), wind rotation and a Gaussian fit to the city plume. Issues with this approach are that the choice of sampling area around the city centre is not standardized and so is prone to subjective area selection and the Gaussian fit often fails or yields non-physical best-fit parameters. Here we address these issues by applying 54 sampling areas to isolated cities. We test our method with TROPOspheric Monitoring Instrument (TROPOMI) NO_2 observations for 2019 over 19 large, isolated cities in South and Southeast Asia that lack contemporary, publicly available bottom-up emissions estimates.

Annual NO_x emissions, obtained for all 19 cities, are < 73 Gg NO_x as NO_2 a^{-1} for most cities, between 73-145 Gg NO_x as NO_2 a^{-1} for Karachi, Delhi, and Jakarta and > 145 Gg NO_x as NO_2 a^{-1} for Bangkok, Dhaka, and Singapore. The overall uncertainty in the annual emissions is 30-60%. Our emissions estimates are in general ~27% more than past studies that use a single sampling area, due to differences in satellite data products and months targeted. The latter we suggest may lead to biases, as the top-down emissions estimate does not properly account for seasonality in photochemical loss of NO_x. Relative differences between our top-down estimates and a widely used bottom-up inventory are < 50% for 9 of the 19 cities, within 50-100% for Ho Chi Minh City, Jakarta, Delhi, and Colombo, and much greater for Karachi (2.1 times), Islamabad (2.1 times), Lahore (2.4 times), Yangon (3.3 times), Dhaka (6.9 times), and Kabul (11-fold). There is a latitudinal dependence of the size of these discrepancies that we suggest is because the top-down approach also does not properly account for spatial variability in the chemical lifetime of NO_x.

The increased success of deriving NO_x emissions with our updated approach enables us to identify that further development is needed to account for time and space variability in the chemical lifetime of NO_x to fully exploit the top-down approach to interrogate seasonality in emissions, to validate bottom-up emissions, to exploit hourly observations from geostationary instruments, and to inform air quality regulation.

Data and Software Availability

The TROPOMI tropospheric columns for 2019 are publicly available from the S5P-PAL Data Portal (https://data-portal.s5p-pal.com/). GEOS-Chem source codes are preserved on Zenodo by The International GEOS-Chem User Community (2021) for GCClassic version 13.3.4 and by The International GEOS-Chem User Community (2022) for GCHP version 13.4.1.

Author Contributions

GL developed the methodology, GL and EAM processed, analysed and interpreted the data. GL and EAM prepared the manuscript. KV assisted in data collection and analysis. RPH and DZ conducted the GEOS-Chem simulations (RPH: GCClassic; DZ: GCHP). RVM contributed to the methodology. SG contributed to interpretation of the results. All co-authors provided editorial input.

Conflicts of interest

The authors declare there are no conflicts of interest.

Acknowledgements

This research has been supported by the European Research Council under the European Union's Horizon 2020 research and innovation programme (through the Starting Grant awarded to Eloise A. Marais, UpTrop; grant no. 851854). GL is grateful for a PhD studentship funded by the China Scholarship Council. RVM acknowledges support from NASA Grant 80NSSC21K0508.

References

Beirle, S., Boersma, K. F., Platt, U., Lawrence, M. G., & Wagner, T. (2011), Megacity Emissions and Lifetimes of Nitrogen Oxides Probed from Space, *Science*, *333*(6050), 1737-1739, doi:10.1126/science.1207824.

Crippa, M., Guizzardi, D., Butler, T., Keating, T., Wu, R., Kaminski, J., et al. (2023), The HTAP_v3 emission mosaic: merging regional and globalmonthly emissions (2000-2018) to support air quality modelling and policies, *Earth System Science Data*, *15*(6), 2667-2694, doi:10.5194/essd-15-2667-2023.

Curier, R. L., Kranenburg, R., Segers, A. S., Timmermans, R. M. A., & Schaap, M. (2014), Synergistic use of OMI NO_2 tropospheric columns and LOTOS-EUROS to evaluate the NO_x emission trends across Europe, *Remote Sensing of Environment*, *149*, 58-69, doi:10.1016/j.rse.2014.03.032.

de Foy, B., Wilkins, J. L., Lu, Z. F., Streets, D. G., & Duncan, B. N. (2014), Model evaluation of methods for estimating surface emissions and chemical lifetimes from satellite data, *Atmospheric Environment*, *98*, 66-77, doi:10.1016/j.atmosenv.2014.08.051.

de Foy, B., Lu, Z. F., & Streets, D. G. (2016), Satellite NO_2 retrievals suggest China has exceeded its NO_x reduction goals from the twelfth Five-Year Plan, *Scientific Reports*, *6*, 9, doi:10.1038/srep35912.

Eastham, S. D., Long, M. S., Keller, C. A., Lundgren, E., Yantosca, R. M., Zhuang, J., et al. (2018), GEOS-Chem High Performance (GCHP v11-02c): a next-generation implementation of the GEOS-Chem chemical transport model for massively parallel applications, *Geoscientific Model Development*, *11*(7), 2941-2953, doi:10.5194/gmd-11-2941-2018.

Eskes, H., van Geffen, J., Sneep, M., Veefkind, P., Niemeijer, S., & Zehner, C. (2021), S5P Nitrogen Dioxide v02.03.01 intermediate reprocessing on the S5P-PAL system: Readme file.

Goldberg, D. L., Lu, Z. F., Oda, T., Lamsal, L. N., Liu, F., Griffin, D., et al. (2019a), Exploiting OMI NO_2 satellite observations to infer fossil-fuel CO_2 emissions from US megacities, *Science of the Total Environment*, *695*, 9, doi:10.1016/j.scitotenv.2019.133805.

Goldberg, D. L., Lu, Z. F., Streets, D. G., de Foy, B., Griffin, D., McLinden, C. A., et al. (2019b), Enhanced Capabilities of TROPOMI NO_2: Estimating NO_x from North American Cities and Power Plants, *Environmental Science & Technology*, *53*(21), 12594-12601, doi:10.1021/acs.est.9b04488.

Goldberg, D. L., Anenberg, S. C., Lu, Z. F., Streets, D. G., Lamsal, L. N., McDuffie, E. E., & Smith, S. J. (2021), Urban NO_x emissions around the world declined faster than anticipated between 2005 and 2019, *Environmental Research Letters*, *16*(11), 11, doi:10.1088/1748-9326/ac2c34.

Grulke, N. E., & Heath, R. L. (2020), Ozone effects on plants in natural ecosystems, *Plant Biology*, *22*, 12-37, doi:10.1111/plb.12971.

Hoornweg, D., & Pope, K. (2017), Population predictions for the world's largest cities in the 21st century, *Environment and Urbanization*, *29*(1), 195-216, doi:10.1177/0956247816663557.

Kurokawa, J., & Ohara, T. (2020), Long-term historical trends in air pollutant emissions in Asia: Regional Emission inventory in ASia (REAS) version 3, *Atmospheric Chemistry and Physics*, *20*(21), 12761-12793, doi:10.5194/acp-20-12761-2020.

Lange, K., Richter, A., & Burrows, J. P. (2022), Variability of nitrogen oxide emission fluxes and lifetimes estimated from Sentinel-5P TROPOMI observations, *Atmospheric Chemistry and Physics*, *22*(4), 2745-2767, doi:10.5194/acp-22-2745-2022.

Laughner, J. L., & Cohen, R. C. (2019), Direct observation of changing NO_x lifetime in North American cities, *Science*, *366*(6466), 723-+, doi:10.1126/science.aax6832.

Lelieveld, J., Evans, J. S., Fnais, M., Giannadaki, D., & Pozzer, A. (2015), The contribution of outdoor air pollution sources to premature mortality on a global scale, *Nature*, *525*(7569), 367-+, doi:10.1038/nature15371.

Li, M., Zhang, Q., Kurokawa, J., Woo, J. H., He, K. B., Lu, Z. F., et al. (2017), MIX: a mosaic Asian anthropogenic emission inventory under the international collaboration framework of the MICS-Asia and HTAP, *Atmospheric Chemistry and Physics*, *17*(2), 935-963, doi:10.5194/acp-17-935-2017.

Lin, H. P., Jacob, D. J., Lundgren, E. W., Sulprizio, M. P., Keller, C. A., Fritz, T. M., et al. (2021), Harmonized Emissions Component (HEMCO) 3.0 as a versatile emissions component for atmospheric models: application in the GEOS-Chem, NASA GEOS, WRF-GC, CESM2, NOAA GEFS-Aerosol, and NOAA UFS models, *Geoscientific Model Development*, *14*(9), 5487-5506, doi:10.5194/gmd-14-5487-2021.

Liu, F., Tao, Z. N., Beirle, S., Joiner, J., Yoshida, Y., Smith, S. J., et al. (2022), A new method for inferring city emissions and lifetimes of nitrogen oxides from high-resolution nitrogen dioxide observations: a model study, *Atmospheric Chemistry and Physics*, *22*(2), 1333-1349, doi:10.5194/acp-22-1333-2022.

Lorente, A., Boersma, K. F., Eskes, H. J., Veefkind, J. P., van Geffen, J., de Zeeuw, M. B., et al. (2019), Quantification of nitrogen oxides emissions from build-up of pollution over Paris with TROPOMI, *Scientific Reports*, *9*, 10, doi:10.1038/s41598-019-56428-5.

Lu, Z., Streets, D. G., de Foy, B., Lamsal, L. N., Duncan, B. N., & Xing, J. (2015), Emissions of nitrogen oxides from US urban areas: estimation from Ozone Monitoring Instrument retrievals for 2005-2014, *Atmospheric Chemistry and Physics*, *15*(18), 10367-10383, doi:10.5194/acp-15-10367-2015.

Luo, L., Wu, Y. F., Xiao, H. Y., Zhang, R. J., Lin, H., Zhang, X. L., & Kao, S. J. (2019), Origins of aerosol nitrate in Beijing during late winter through spring, *Science of the Total Environment*, *653*, 776-782, doi:10.1016/j.scitotenv.2018.10.306.

Marais, E. A., Kelly, J. M., Vohra, K., Li, Y. F., Lu, G. D., Hina, N., & Rowe, E. C. (2023), Impact of Legislated and Best Available Emission Control Measures on UK Particulate Matter Pollution, Premature Mortality, and Nitrogen-Sensitive Habitats, *Geohealth*, *7*(10), doi:10.1029/2023gh000910.

Marvin, M. R., Palmer, P. I., Latter, B. G., Siddans, R., Kerridge, B. J., Latif, M. T., & Khan, M. F. (2021), Photochemical environment over Southeast Asia primed for hazardous ozone levels with influx of nitrogen oxides from seasonal biomass burning, *Atmospheric Chemistry and Physics*, *21*(3), 1917-1935, doi:10.5194/acp-21-1917-2021.

McDuffie, E. E., Smith, S. J., O'Rourke, P., Tibrewal, K., Venkataraman, C., Marais, E. A., et al. (2020), A global anthropogenic emission inventory of atmospheric pollutants from sector- and fuel-specific sources (1970-2017): an application of the Community Emissions Data System (CEDS), *Earth System Science Data*, *12*(4), 3413-3442, doi:10.5194/essd-12-3413-2020.

Miyazaki, K., Eskes, H. J., Sudo, K., & Zhang, C. (2014), Global lightning NO_x production estimated by an assimilation of multiple satellite data sets, *Atmospheric Chemistry and Physics*, *14*(7), 3277-3305, doi:10.5194/acp-14-3277-2014.

Murray, L. T., Jacob, D. J., Logan, J. A., Hudman, R. C., & Koshak, W. J. (2012), Optimized regional and interannual variability of lightning in a global chemical transport model constrained by LIS/OTD satellite data, *Journal of Geophysical Research-Atmospheres*, *117*, 14, doi:10.1029/2012jd017934.

Pope, R. J., Kelly, R., Marais, E. A., Graham, A. M., Wilson, C., Harrison, J. J., et al. (2022), Exploiting satellite measurements to explore uncertainties in UK bottom-up NO_x emission estimates, *Atmospheric Chemistry and Physics*, *22*(7), 4323-4338, doi:10.5194/acp-22-4323-2022.

Potts, D. A., Marais, E. A., Boesch, H., Pope, R. J., Lee, J., Drysdale, W., et al. (2021), Diagnosing air quality changes in the UK during the COVID-19 lockdown using TROPOMI and GEOS-Chem, *Environmental Research Letters*, *16*(5), doi:10.1088/1748-9326/abde5d.

Randerson, J. T., Van Der Werf, G. R., Giglio, L., Collatz, G. J., & Kasibhatla, P. S. (2017), Global Fire Emissions Database, Version 4.1 (GFEDv4), 10.3334/ORNLDAAC/1293.

Shah, V., Jacob, D. J., Li, K., Silvern, R. F., Zhai, S., Liu, M., et al. (2020), Effect of changing NO_x lifetime on the seasonality and long-term trends of satellite-observed tropospheric NO_2 columns over China, *Atmospheric Chemistry and Physics*, *20*(3), 1483-1495, doi:10.5194/acp-20-1483-2020.

Sillman, S. (1999), The relation between ozone, NO_x and hydrocarbons in urban and polluted rural environments, *Atmospheric Environment*, *33*(12), 1821-1845, doi:10.1016/s1352-2310(98)00345-8.

Silvern, R. F., Jacob, D. J., Mickley, L. J., Sulprizio, M. P., Travis, K. R., Marais, E. A., et al. (2019), Using satellite observations of tropospheric NO_2 columns to infer long-term trends in US NO_x emissions: the importance of accounting for the free tropospheric NO_2 background, *Atmospheric Chemistry and Physics*, *19*(13), 8863-8878, doi:10.5194/acp-19-8863-2019.

Sun, K., Zhu, L., Cady-Pereira, K., Miller, C. C., Chance, K., Clarisse, L., et al. (2018), A physics-based approach to oversample multi-satellite, multispecies observations to a common grid, *Atmospheric Measurement Techniques*, *11*(12), 6679-6701, doi:10.5194/amt-11-6679-2018.

The International GEOS-Chem User Community (2021). *GCClassic version 13.3.4. Zenodo [software]*. doi:https://doi.org/10.5281/zenodo.5764874.

The International GEOS-Chem User Community (2022). *GCHP version 13.4.1. Zenodo [software]*. doi:https://doi.org/10.5281/zenodo.6564711.

Tzortziou, M., Kwong, C. F., Goldberg, D., Schiferl, L., Commane, R., Abuhassan, N., et al. (2022), Declines and peaks in NO_2 pollution during the multiple waves of the COVID-19 pandemic in the New York metropolitan area, *Atmospheric Chemistry and Physics*, *22*(4), 2399-2417, doi:10.5194/acp-22-2399-2022.

Valin, L. C., Russell, A. R., & Cohen, R. C. (2013), Variations of OH radical in an urban plume inferred from NO_2 column measurements, *Geophysical Research Letters*, *40*(9), 1856-1860, doi:10.1002/grl.50267.

van Geffen, J., Boersma, K. F., Eskesl, H., Sneep, M., ter Linden, M., Zara, M., & Veefkind, J. P. (2020), S5P TROPOMI NO_2 slant column retrieval: method, stability, uncertainties and comparisons with OMI, *Atmospheric Measurement Techniques*, *13*(3), 1315-1335, doi:10.5194/amt-13-1315-2020.

van Geffen, J., Eskes, H., Boersma, K. F., & Veefkind, P. (2021), TROPOMI ATBD of the total and tropospheric NO_2 data products (issue 2.2.0), Royal Netherlands Meteorological Institute (KNMI), De Bilt, the Netherlands.

van Geffen, J., Eskes, H., Compernolle, S., Pinardi, G., Verhoelst, T., Lambert, J.-C., et al. (2022), Sentinel-5P TROPOMI NO_2 retrieval: impact of version v2.2 improvements and comparisons with OMI and ground-based data, *Atmospheric Measurement Techniques*, *15*(7), 2037-2060, doi:10.5194/amt-15-2037-2022.

Verstraeten, W. W., Boersma, K. F., Douros, J., Williams, J. E., Eskes, H., Liu, F., et al. (2018), Top-Down NO_x Emissions of European Cities Based on the Downwind Plume of Modelled and Space-Borne Tropospheric NO_2 Columns, *Sensors*, *18*(9), doi:10.3390/s18092893.

Vohra, K., Marais, E. A., Suckra, S., Kramer, L., Bloss, W. J., Sahu, R., et al. (2021), Long-term trends in air quality in major cities in the UK and India: a view from space, *Atmospheric Chemistry and Physics*, *21*(8), 6275-6296, doi:10.5194/acp-21-6275-2021.

Vohra, K., Marais, E. A., Bloss, W. J., Schwartz, J., Mickley, L. J., Van Damme, M., et al. (2022), Rapid rise in premature mortality due to anthropogenic air pollution in fast-growing tropical cities from 2005 to 2018, *Science Advances*, *8*(14), 13, doi:10.1126/sciadv.abm4435.

Weng, H. J., Lin, J. T., Martin, R., Millet, D. B., Jaeglé, L., Ridley, D., et al. (2020), Global high-resolution emissions of soil NO_x, sea salt aerosols, and biogenic volatile organic compounds, *Scientific Data*, *7*(1), 15, doi:10.1038/s41597-020-0488-5.

Wu, N., Geng, G. N., Yan, L., Bi, J. Z., Li, Y. S., Tong, D., et al. (2021), Improved spatial representation of a highly resolved emission inventory in China: evidence from TROPOMI measurements, *Environmental Research Letters*, *16*(8), 11, doi:10.1088/1748-9326/ac175f.

Yue, X., Unger, N., Harper, K., Xia, X. G., Liao, H., Zhu, T., et al. (2017), Ozone and haze pollution weakens net primary productivity in China, *Atmospheric Chemistry and Physics*, *17*(9), 6073-6089, doi:10.5194/acp-17-6073-2017.

Zhang, L., Jacob, D. J., Knipping, E. M., Kumar, N., Munger, J. W., Carouge, C. C., et al. (2012), Nitrogen deposition to the United States: distribution, sources, and processes, *Atmospheric Chemistry and Physics*, *12*(10), 4539-4554, doi:10.5194/acp-12-4539-2012.